JOURNAL OF THEORETICAL AND APPLIED MECHANICS
62, 1, pp. 19-30, Warsaw 2024
https://doi.org/10.15632/jtam-pl/174870

ULTRAHIGH FREQUENCY VIBRATION CONTROL IN A PIEZOELECTRIC PHONONIC CRYSTAL BEAM AT THE NANOSCALE CONSIDERING SURFACE EFFECTS

Zexin Zhang, Denghui Qian
School of Naval Architecture and Ocean Engineering, Jiangsu University of Science and Technology, Zhenjiang, China
corresponding author Denghui Qian: e-mail: dhqian@just.edu.cn
Long Ren, Qi Wang
China Nanhu Academy of Electronics and Information Technology, Jiaxing, China

In this paper, a piezoelectric phononic crystal beam at the nanoscale has been mechanically modeled by using the surface piezoelectric theory. The band gap has been calculated by the plane wave expansion method and the band gap structure picture has been analyzed. The influence of electromechanical coupling effects, surface effects and geometry on the band gap properties are discussed separately. This study contributes positively to the design and active control of nanoelectromechanical systems.

Keywords: phononic crystal, nanobeam, surface effects, electromechanical coupling effects

1. Introduction

In 1992, M.M. Sigalas and E.N. Economou first confirmed theoretically that the three--dimensional periodic lattice structure formed by filling a certain matrix material in a spherical scatterer has characteristics of an elastic wave/acoustic wave band gap. Compared with the electromagnetic wave band gap of a photonic crystal, they defined a concept of an elastic wave/acoustic wave band gap phononic crystal (Sigalas and Economou, 1992). Due to its band gap, defect state and other characteristics, scholars have carried out extensive research on phononic crystals in the fields of ship and ocean, aerospace engineering and construction (Yin *et al.*, 2022), such as low-frequency vibration isolation/sound insulation/absorption (Chu *et al.*, 2023; Zou *et al.*, 2023; Zuo *et al.*, 2022), subwavelength acoustic focusing (Yang *et al.*, 2022; Yao *et al.*, 2021), acoustic/elastic wave cloak design (Ghoreshi and Bahrami, 2022), ultrahigh frequency resonators (Yao *et al.*, 2021), wave filters (Lee *et al.*, 2023), etc.

In recent years, scholars have done a lot of research between phononic crystal band gap regulation and metamaterial design, such as introducing other physical fields (magnetic field, electric field, temperature, etc.) to regulate the nature of the phononic band gap, which can realize dynamic control of acoustic waves, such as piezomagnetic phononic crystals, piezoelectric phononic crystals, magneto-electroelastic phononic crystals and so on (Qian *et al.*, 2022). Among them, piezoelectric materials as functional materials, such as piezoelectric ceramics, piezoelectric crystals and piezoelectric polymers, have characteristics of a fast response, more flexible and intelligent, and its principle is mutual conversion between mechanical energy and electrical energy, which can be used to actively regulate the band gap by an electric field, and it is widely used in the fabrication of electromechanical transducers and acoustic devices with acoustic-electric effects. The main types of piezoelectric phononic crystals are single, embedded piezoelectric/elastic composite, and externally attached piezoelectric film/elastic structure composite type.

The above phononic crystals are all studied under the macroscopic scale size, with continuous development of nano-preparation technology. The study of the structure of materials with nanoscale size tends to be popular, and a number of works on the study of the structure of nano-phononic crystals emerged (Chen *et al.*, 2017; Huang and Yu, 2006; Yan and Jiang, 2011; Zhen *et al.*, 2012). The band gap of phononic crystals has also been shifted from hertz (Hz), megahertz (MHz) to gigahertz (GHz), and terahertz (THz).

Nanomaterials exhibit several unique effects due to their small size and specific properties. These effects include the surface effect, small size effect, quantum size effect, and macro quantum tunneling effect (Du *et al.*, 2000). The classical continuum theory in the macro scale mechanical model falls short in accurate describing the behavior of nanomaterials due to size-dependent effects observed in them.

However, many scholars have modified the classical mechanics theory and proposed higher-order theories, such as: micropolar theory (Surana *et al.*, 2017), nonlocal elastic continuum theory (Eringen and Edelen, 1972), surface elasticity theory (Gurtin *et al.*, 1998), strain gradient theory (Aifantis, 1999), and modified coupled stress theory (Yang *et al.*, 2002). The surface/interface of nanostructured scatterers has different elastic characteristics from the internal bulk material. Gurtin and Murdoch (1975) established a surface/interface elastic model which abstracts the surface/interface into a thickness-independent elastic film that is intimately bound to the internal material and does not slip. The theoretical model can be used to analyze the surface/interface effect of nanostructured scatterers.

For piezoelectric nanomaterials, the traditional surface elastic model has some limitations. Piezoelectric nanomaterials exhibit surface piezoelectric and dielectric effects, which are key factors overlooked by traditional surface elastic models. To address these limitations, Huang and Yu (2006) proposed a surface piezoelectric model that incorporates the effects of surface piezoelectricity, elasticity, and dielectricity. Their approach to this model allowed for an examination of the stress and charge response pertaining to the surface piezoelectric effect in piezoelectric rings. Notably, the outcomes of their investigation unveiled the substantial influence of surface piezoelectricity on electromechanical characteristics of piezoelectric nanostructures.

Moreover, vibration and buckling characteristics of piezoelectric nanobeams were explored by Yan and Jiang (2011), taking into account the influence of surface effects. Their research underscored the paramount role of surface residual stress and surface piezoelectricity, which revealed a substantial influence over the resonant frequency and critical buckling potential. In comparison, the impact of surface elasticity was comparatively less significant. This implies that the surface piezoelectric effect and surface residual stress should be carefully considered in the design and analysis of nanoscale piezoelectric structures.

Overall, these studies provide a valuable theoretical support for the application of nanoscale piezoelectric materials. By considering the surface piezoelectric, surface elastic, and surface dielectric effects, researchers can gain a more comprehensive understanding of the electromechanical behavior of piezoelectric nanomaterials and optimize their performance in various applications.

In recent years, researchers have made a significant progress in the development of calculation methods to analyze the band gap structure of phononic crystals. At present, the commonly used methods are: plane wave expansion method (PWE) (Zuo *et al.*, 2022), lumped mass method (Kong *et al.*, 2023), finite difference time domain (FDTD) method (Cao *et al.*, 2004), finite element method (FEM) (Lu *et al.*, 2022). As a mature method for numerical simulation of mechanical systems, the finite element method has a worked well with periodic structures and has also been successfully applied to the calculation of one-, two- and three-dimensional structures. However, it produces a large number of node degrees of freedom, which increases the computation amount and requires huge cost. The calculation amount of PWE is much smaller than that of FEM, and its calculation results have also been verified to be consistent with FEM (Qian and

Shi, 2017). The PWE method transforms the band structure calculation into the solution of a generalized eigenvalue problem by expanding the material and displacement field of the periodic structure into Fourier series and combining the Bloch theorem.

In this paper, a mechanical model of a circular cross-section piezoelectric phononic crystal nanobeam is proposed by considering the surface effect. Through a combination of PWE, Euler-Bernoulli beam theory and surface elasticity theory, the control equation for a circular cross section phononic crystal nanobeam is obtained. It proposes a computational approach to study the band gap structure, and explores the effects of mechanical-electrical coupling, surface effect, and geometric size on the first two orders of the band gap in phononic crystals through band gap calculations and analysis of the band structure diagram.

2. Model and method

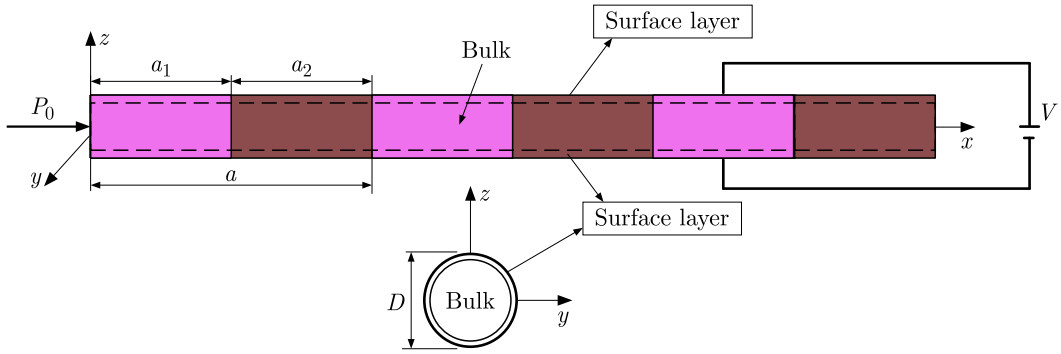

Fig. 1. A model of a piezoelectric phononic crystal nanobeam with surface effects

This paper discusses the investigation of a circular piezoelectric nanophononic crystal beam. The beam structure is composed of alternating cycles of a piezoelectric material, specifically PZT-5H, and an elastic material known as an epoxy resin. The primary focus of this study is to analyze the properties and behavior of this unique crystal beam configuration. A Cartesian coordinate system is shown in Fig. 1. The x-axis represents the axial direction, the y-axis represents the width direction, and the z-axis represents the height direction. In the crystal beam structure, an electric field V is applied to the epoxy resin. In addition, an applied axial force P_0 is considered. These external inputs introduce mechanical-electrical coupling effects into the system. The lattice parameter a has the following definition

$$a = a_1 + a_2 \tag{2.1}$$

where a_1, a_2 are sizes of the piezoelectric material PZT-5H and the elastic material epoxy resin in a cell.

In the proposed analysis, the circular cross section of the piezoelectric nano-phononic crystal beam has a diameter of D. In this particular study, material interface effects are neglected, but the surface effects are still considered and assumed to exist on the surface of the beam. To reflect these surface effects, the beam structure is divided into a surface layer and a block layer. However, the thickness of the surface layer is usually ignored, so the beam cross-section is circular.

From the Euler-Bernoulli beam theory, the axial strain ε_x and deflection $w(x,t)$ at any point in the beam are defined as

$$\varepsilon_x = -z\frac{\partial^2 w(x,t)}{\partial x^2} \tag{2.2}$$

The electric field strength E_z in the direction z is represented by the potential Φ as

$$E_z = -\frac{\partial \Phi}{\partial z} \tag{2.3}$$

The block eigenstructure equation of PZT-5H is expressed as

$$\sigma_x = c_{11}\varepsilon_x - e_{31}E_z \qquad D_z = e_{31}\varepsilon_x + \kappa_{33}E_z \tag{2.4}$$

where σ_x denotes the axial stress and D_z denotes the surface potential shift in the z-direction. c_{11}, e_{31} and κ_{33} denote the modulus of elasticity, piezoelectricity constant, and dielectric constant, respectively.

According to the potential shift boundary condition in electromagnetic theory, the normal potential shifts can be equal. In the Gurtin-Murdoch surface theory model, the surface layer potential shifts and the interface potential shifts are the same, so the PZT-5H surface layer constitutive equation can be derived:

$$\sigma_x^s = \sigma_x^0 + c_{11}^s\varepsilon_x^s - e_{31}^s E_z^s \qquad D_z^s = D_z^0 \tag{2.5}$$

where σ_x^s and σ_x^0 denote the axial surface stress and residual surface stress, respectively. D_z^s and D_z^0 denote the surface potential shift and residual surface potential shift, respectively. E_z^s denotes the surface electric field strength in the z-direction, so $E_z^s = E_z$ due to equality of the electric field strengths of the surface layer and the bulk layer. ε_x^s denotes the surface strain. c_{11}^s and e_{31}^s denote the surface Young's elastic modulus and the surface piezoelectric constant.

Disregarding the free charge, it follows from Gauss' theorem

$$\frac{\partial D_z}{\partial z} = 0 \tag{2.6}$$

Substituting Eqs. (2.2) and (2.3) into $(2.4)_2$ and (2.6)

$$\Phi = -\frac{1}{2}z^2\frac{e_{31}}{\kappa_{33}}\frac{\partial^2 w(x,t)}{\partial x^2} + zf_1(x,y) + f_2(x,y) \tag{2.7}$$

Considering the electric field boundary conditions $\Phi(-D/2) = 0$ and $\Phi(D/2) = V$, the electric potential is obtained as

$$\Phi = -\frac{e_{31}}{2\kappa_{33}}\frac{\partial^2 w(x,t)}{\partial x^2}\Big(z^2 - \frac{D^2}{4}\Big) + \frac{V}{D}z + \frac{V}{2} \tag{2.8}$$

Substituting Eq. (2.8) into (2.3), the electric field strength E_z can be expressed as

$$E_z = z\frac{e_{31}}{\kappa_{33}}\frac{\partial^2 w(x,t)}{\partial x^2} - \frac{V}{D} \tag{2.9}$$

Substituting Eqs. (2.8) and (2.9) into $(2.4)_1$ and $(2.5)_1$, the axial stresses in the PZT-5H block and surface layer can be expressed as

$$\begin{aligned} \sigma_x &= e_{31}\frac{V}{D} - \Big(c_{11} + \frac{e_{31}^2}{\kappa_{33}}\Big)z\frac{\partial^2 w(x,t)}{\partial x^2} \\ \sigma_x^s &= \sigma_x^0 + e_{31}^s\frac{V}{D} - \Big(c_{11}^s + \frac{e_{31}^s e_{31}}{\kappa_{33}}\Big)z\frac{\partial^2 w(x,t)}{\partial x^2} \end{aligned} \tag{2.10}$$

For the block part of the epoxy, the eigenstructure equation can be described as

$$\sigma_x = E\varepsilon_x \tag{2.11}$$

where E denotes the elastic modulus.

The epoxy surface layer portion of the epoxy resin, whose intrinsic formula is expressed as

$$\sigma_x^s = \sigma_x^0 + E^s \varepsilon_x^s \tag{2.12}$$

where E^S denotes the surface elastic modulus.

Substituting Eq. (2.2) into (2.11) and (2.12), the axial stress of the epoxy can be defined by bending deflection as

$$\sigma_x = -Ez\frac{\partial^2 w(x,t)}{\partial x^2} \qquad \sigma_x^s = \sigma_X^0 - E^s z\frac{\partial^2 w(x,t)}{\partial x^2} \tag{2.13}$$

All surface layer and block parameters have a certain correspondence

$$p_s \leftrightarrow l_s p_b \tag{2.14}$$

where p_s, p_b are the respective surface layer and block parameters, and l_s are the material internal parameters.

Derived from the generalized Young-Laplace equation and the corresponding formula (Yan and Jiang, 2011), the vibration control equation of the nanobeam considering surface effect can be expressed as

$$\frac{\partial^2 M}{\partial x^2} - P\frac{\partial^2 w(x,t)}{\partial x^2} - \frac{\partial}{\partial x}\int_C T_x z \, dC - \int_C T_z \, dC = -\rho S\frac{\partial^2 w(x,t)}{\partial t^2} \tag{2.15}$$

The corresponding parameters are shown as follows:

$$M = -\int_S \sigma_x z \, dS \qquad P = P_0 + \int_S \sigma_x \, dS \qquad T_x = \frac{\partial \sigma_x^s}{\partial x} \qquad T_z = \frac{\sigma_x^s}{R_c} \tag{2.16}$$

where M is the bending moment, P is the axial force, T_x and T_z are the traction jumps caused by surface stress, T_z only acts on the top and bottom of the beam. C and S represent the circumference and area of the interface, ρ is density of the material, and R_c is curvature.

For the z-direction surface tension T_z of the top and bottom surfaces of the beam, in the calculation of the circular section (Qian, 2018), it is regarded as a square section with an equal area. In this paper, it is improved: the z-axis is taken as the central axis, the left and right sweeps 45°, and the formed area is regarded as the upper and lower surface (as shown in Fig. 2). To obtain surface tension in the z-direction, integration along this boundary is performed.

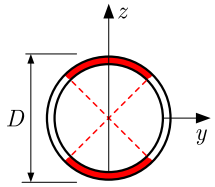

Fig. 2. Surface tension T_z integral region (red)

Substituting the above equations, the vibration control equations for piezoelectric and elastic nanobeams considering surface effects can therefore be uniformly expressed as

$$\frac{\partial^2}{\partial x^2}\Big(m(x)\frac{\partial^2 w(x)}{\partial x^2}\Big) - n(x)\frac{\partial^2 w(x)}{\partial x^2} = \omega^2 p(x) w(x) \tag{2.17}$$

where $m(x) = (m_1(x), m_2(x))$, $n(x) = (n_1(x), n_1(x))$, $p(x) = (p_1(x), p_2(x))$

$$\begin{aligned} &m_1(x) = \frac{\pi D^4}{64}\overline{c} + \frac{\pi D^3}{8}\overline{c}^s \qquad m_2(x) = \frac{\pi D^4}{64}E + \frac{\pi D^3}{8}E^s \\ &n_1(x) = \frac{\pi D}{4}\Big(\sigma_x^0 + e_{31}^s\frac{V}{D} + 2e_{31}V\Big) + P_0 \qquad n_2(x) = \frac{\pi D}{4}\sigma_x^0 + P_0 \\ &p_1(x) = \rho_1 A \qquad p_2(x) = \rho_2 A \end{aligned} \tag{2.18}$$

where $\overline{c} = c_{11} + e_{31}^2/\kappa_{33}$, $\overline{c}^s = c_{11}^s + e_{31}^s e_{31}/\kappa_{33}$, ρ_1, ρ_2 represent density of the PZT-5H and epoxy resin.

Due to the axial periodicity of the structural material, $M(x)$, $N(x)$ and $P(x)$ are all periodic functions in the x-direction, and can therefore be expanded into a Fourier series. Here, three functions can be expressed uniformly by $g(x)$

$$g(x) = \sum_G g(G) \mathrm{e}^{\mathrm{i}Gx} \tag{2.19}$$

where G is the reciprocal lattice vector and $g(G)$ is the Fourier expansion coefficient which can be defined as

$$g(G) = \begin{cases} g_A f + g_B(1-f) & \text{fox} \quad G = 0 \\ (g_A - g_B)\Upsilon(G) & \text{fox} \quad G \neq 0 \end{cases} \tag{2.20}$$

where g_A, g_B are the corresponding coefficients of the material, respectively, and $f = a_2/a$ denotes the filling ratio of the epoxy resin to the whole protocell and, in addition, $\Upsilon(G) = f\sin(Ga_2/2)/(Ga_2/2)$ is a structural function, and is only related to the shape of the scatterer epoxy resin.

Due to the periodicity of the structure and Bloch's theorem, the displacement field $w(x)$ can be decomposed as follows

$$w(x) = w_k(x) \mathrm{e}^{\mathrm{i}(kx - \omega t)} \tag{2.21}$$

where k is the Bloch wave vector confined to the first Brillouin zone. The function w_k has the same periodicity as the material parameters and can be expressed as a Fourier series

$$w_k(x) = \sum_{G'} \mathrm{e}^{\mathrm{i}G'x} w_k(G') \tag{2.22}$$

Substituting it into Eq. (2.21), w_k can be defined as

$$w(x) = \mathrm{e}^{-\mathrm{i}\omega t} \sum_{G'} \mathrm{e}^{\mathrm{i}(G'+k)x} w_k(G') \tag{2.23}$$

Substituting Eqs. (2.19) and (2.23) into (2.17) and selecting N inverted lattice vectors for calculation, we can obtain the following equation

$$(\boldsymbol{MG} + \boldsymbol{NG} - \omega^2 \mathbf{PG}) \times \mathbf{w}(\mathbf{G}) = \mathbf{0} \tag{2.24}$$

where

$$\begin{aligned} &[\boldsymbol{MG}]_{ij} = (\mathbf{k} + \mathbf{G}_i)^2 m(\mathbf{G}_i - \mathbf{G}_j)(\mathbf{k} + \mathbf{G}_j)^2 \\ &[\mathbf{NG}]_{ij} = n(\mathbf{G}_i - \mathbf{G}_j)(\mathbf{k} + \mathbf{G}_j)^2 \qquad [\mathbf{PG}]_{ij} = p(\mathbf{G}_i - \mathbf{G}_j) \end{aligned} \tag{2.25}$$

Equation (2.24) is a linear equation for solving the generalized eigenvalues of ω^2. For a given Bloch wave vector $\mathbf{k}$ in the first Brillouin zone, a series of eigenvalues ω_{kn} $(n = 1, 2, \ldots)$ can be obtained. The energy band structure of this piezoelectric nanophononic crystal beam can be obtained when $\mathbf{k}$ varies over $[-\pi/2, \pi/2]$.

3. Numerical results and analyses

3.1. Band structures of PC nanobeams with circular cross sections

The band gap structure of piezoelectric nanophononic crystal beams with a circular cross--section was determined based on the parameters provided in Table 1. The results of energy

Table 1. Bulk material parameters of PZT-5H and epoxy (Yan and Jiang, 2011)

Material	ρ [kg/m^3]	E [GPa]	c_{11} [GPa]	e_{31} [C/m2]	κ_{33} [C/(Vm)]
PZT-5H	7500	–	126	−6.5	$1.3 \cdot 10^{-8}$
Epoxy	1180	76	–	–	–

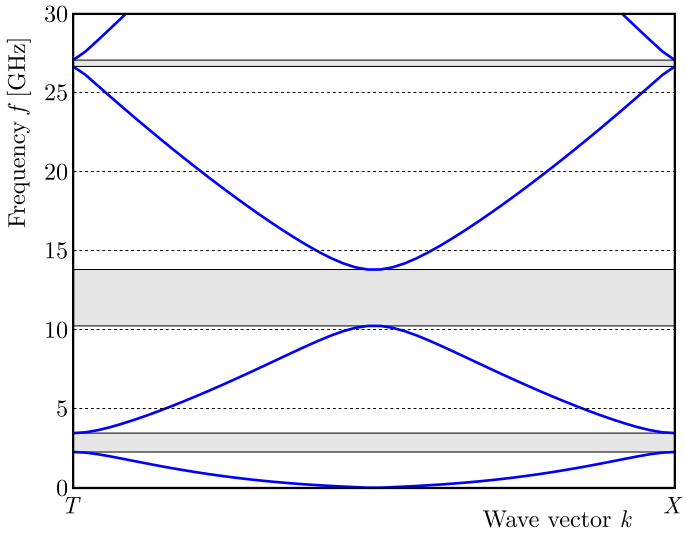

Fig. 3. Band structure of piezoelectric nanophononic crystal beams with a circular cross-section considering surface effects

band structure calculations are illustrated in Fig. 3. The geometric parameters used for the calculations were: $a_1 = a_2 = 50\,\text{nm}$, and $D = 10\,\text{nm}$. The parameters for the surface layer were as follows: $\sigma_x^0 = 1\,\text{N/m}$ and $l_s = 1\,\text{nm}$. The applied voltage was $V = 0.2\,\text{V}$, and the applied axial force was $P_0 = 110^{-8}\,\text{N}$.

As depicted in Fig. 3, there are three fully open band gaps below 30 GHz. In this paper, the characteristics of the first two orders of the band gap are investigated. Specifically, the first-order band gap ranges from 2.2762 Hz to 3.4735 GHz, with a band gap width of 1.913 GHz. The second-order band gap spans from 10.2557 GHz to 13.8244 GHz, with a band gap width of 3.5687 GHz.

3.2. Influence of electromechanical coupling effects on band gap characteristics

As shown in Fig. 4, it illustrates the influence of voltage on the vibration band gap of piezoelectric nanophononic crystal beams with surface effects. The calculation parameters for this analysis are provided in Table 1. From the figure, it can be observed that as the voltage varies from −50 V to 20 V, the starting frequency of the first-order and the second-order band gap decreases continuously and tends to 0. This indicates that the band gap shifts towards lower frequencies as the voltage increases. The width of the first-order and the second-order band gap exhibits non-monotonic behavior. The former initially decreases, then increases, and finally decreases again, ultimately approaching 0. The later shows a gradual increase, reaching a peak, and then decreases until it tends to 0.

As shown in Fig. 5, it illustrates the impact of the applied axial force P_0 on the band gap of piezoelectric nanophononic crystal beams. In Fig. 5, as the axial force varies from $-40 \cdot 10^{-8}\,\text{N}$ to $10 \cdot 10^{-8}\,\text{N}$, the starting frequency of the first two orders of the band gap increases continuously from 0. This indicates that the band gap shifts towards higher frequencies as the axial force increases. Furthermore, the width of the band gap initially increases, then decreases, and finally increases again.

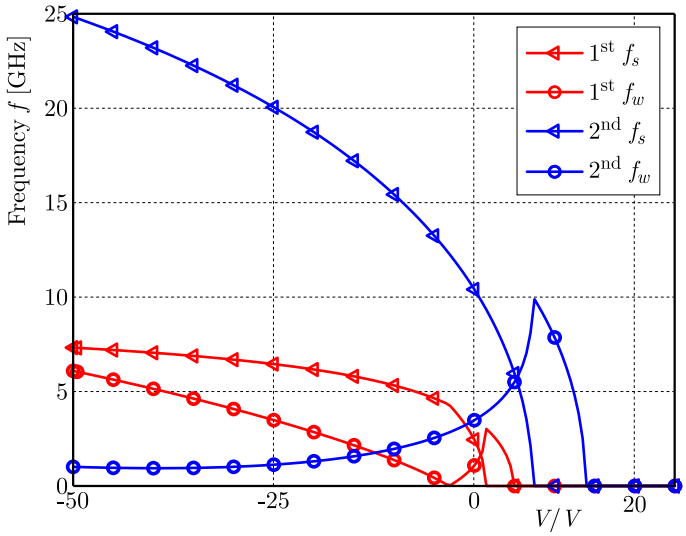

Fig. 4. The influence of voltage V on the band gap

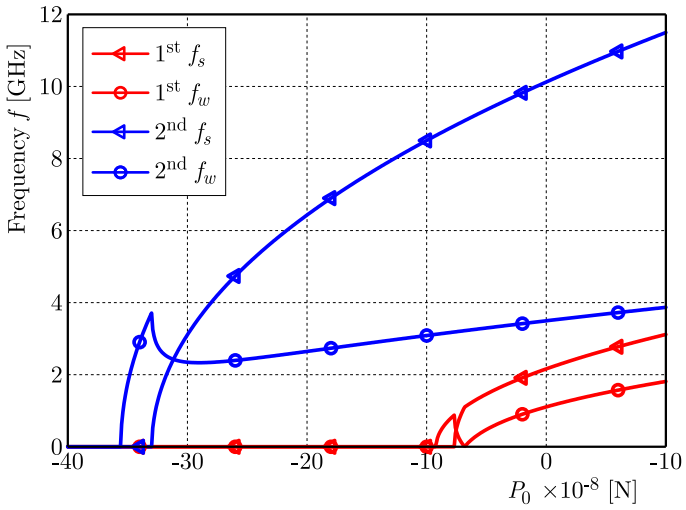

Fig. 5. The influence of the applied axial force P_0 on the band gap

3.3. Influence of surface effects on band gap characteristics

Figure 6 demonstrates the influence of the material characterization length l_s on the band gap of the system. The range of l_s values considered is from 0 nm to 1 nm. From the figure, it is evident that the characterization length l_s exhibits an increasing trend on both the onset frequency and band gap width of the first-order. As the value of l_s increases, the onset frequency of the first-order band gap shifts towards higher frequencies, and the width of the band gap also increases. Similarly, the onset frequency and band gap width of the second-order also show a similar increasing trend with the characterization length l_s. As the value of l_s increases, the onset frequency of the second-order band gap shifts towards higher frequencies, and the width of the band gap also increases.

As shown in Fig. 7, it illustrates the impact of surface residual stress σ_x^0 on the band gap of the system. The range of σ_x^0 values considered is from 0 N/m to 1 N/m. According to the figure, it is evident that the surface residual stress σ_x^0 has a weak increasing trend on both the onset frequency and width of the first-order and the second-order band gap. However, the trend can be approximated as remaining relatively constant within the range of values considered. This indicates that as the surface residual stress σ_x^0 increases within the given range, there is a slight

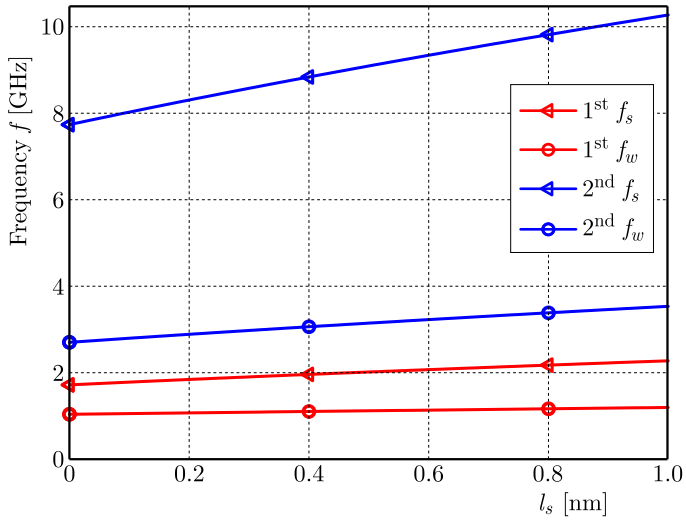

Fig. 6. The influence of the material characterization length l_s on the band gap

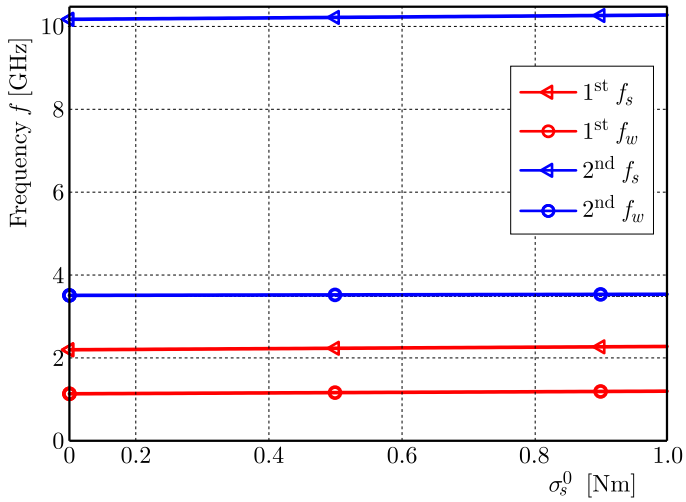

Fig. 7. The influence of the surface residual stress σ_x^0 on the band gap

overall effect on the band gap characteristics. The onset frequency and width of both the first--order and the second-order band gap may experience minimal changes, potentially exhibiting a gradual increase. However, these changes are generally small compared to the range of values considered, and the trend can be approximated as remaining constant.

3.4. Influence of geometric parameters on band gap characteristics

As shown in Fig. 8, it demonstrates the impact of the circular cross-section diameter D of a piezoelectric nanophononic crystal beam on the first-order starting frequency, band gap width, and the second-order starting frequency, band gap width. In this analysis, the diameter D is varied from 0 nm to 25 nm, while other parameters remain consistent with Table 1. From the figure, it can be observed that as the diameter D increases, there is a consistent trend in changes of the first-order and the second-order starting frequencies as well as the band gap widths. Specifically, the values initially decrease and then increase.

Figure 9 depicts the influence of the length ratio a_1/a_2 between the PZT-5H and epoxy resin on the onset frequency and band gap width of the first two orders of the band gap. As the length ratio a_1/a_2 increases, the onset frequency of both the first-order and the second-order band gap

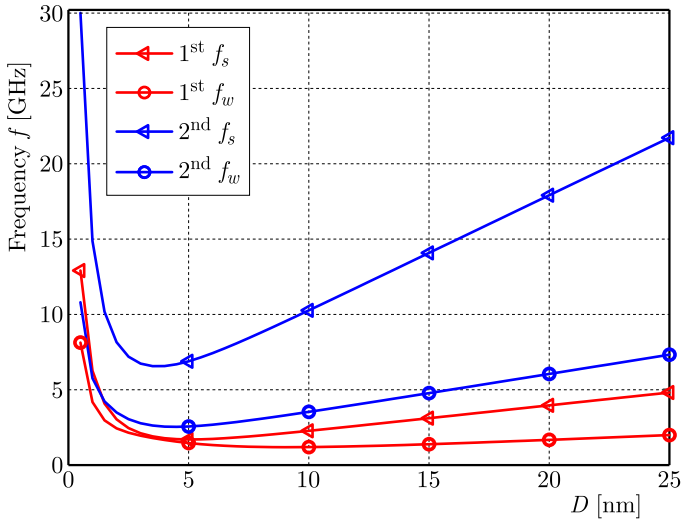

Fig. 8. The influence of the cross-sectional diameter D on the band gap

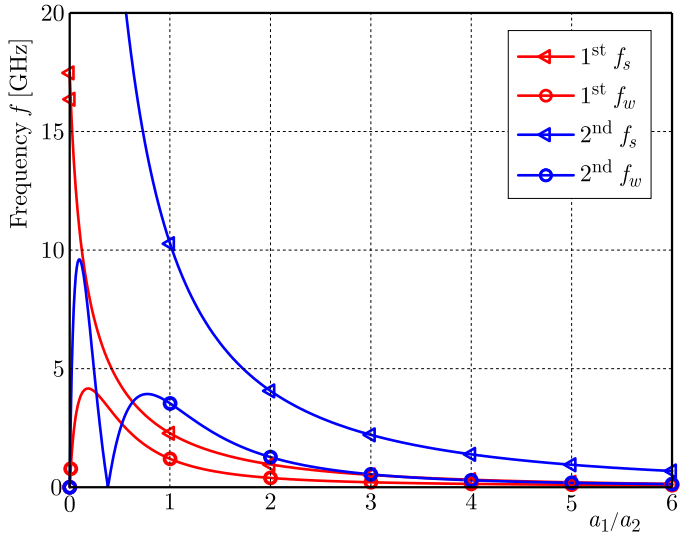

Fig. 9. The influence of a_1/a_2 on the band gap

decreases and tends towards 0. This suggests that a higher length ratio corresponds to lower starting frequencies of the band gaps. Concerning the band gap width, the trend observed for both the first-order and the second-order band gap can be roughly approximated as initially increasing up to a peak, and then decreasing towards 0. This implies that there is an optimal length ratio that maximizes the band gap width for each order of the band gap. It is important to avoid excessive length ratios if a wide band gap width is desired in engineering applications. Instead, designing the length ratio near the peak value can help maximize the band gap width.

4. Conclusions

In this paper, the band gap characteristics of piezoelectric nanophononic crystal beams with circular cross-sections are analyzed and explored in terms of the electromechanical coupling effect, surface effect, and geometry, respectively, and the following conclusions are drawn:

- With an increase of voltage V, the first two orders of the band gap move towards the lower frequency. The first order band gap shows a minus increase and tends to 0, the second

order band gap increases first and then decreases and tends to 0. With an increase of the applied axial force P_0, the first two orders of the band gap move in the lower frequency direction, and the width of the band gap shows the tendency of an increase and decrease.

- The increase of the material characterization length l_s makes the starting frequency of the band gap move in the high frequency direction, and the bandwidth increases. The increase in the surface residual stress σ_x^0 has a smaller effect on the band gap characteristics and can be approximated as remaining relatively stable.
- As the diameter D of the circular cross-section increases, the onset frequency and width of the band gap of the first two orders both decrease and then increase. The increase of the length ratio a_1/a_2 makes the onset frequency of the first two orders of the band gap decrease and tend to zero, which means that a higher length ratio corresponds to a lower onset frequency of the band gap, and the width of the first two orders of the band gap exhibits an increase and then decreases and tends to zero.

Acknowledgments

This research was supported by the National Natural Science Foundation of China (No. 52301373), the Young Elite Scientists Sponsorship Program by CAST (2022QNRC001) and the Natural Science Foundation of Jiangsu Higher Education Institutions of China (No. 22KJB580005).

References

1. Aifantis E.C., 1999, Strain gradient interpretation of size effects, *International Journal of Fracture*, **95**, 299-314
2. Cao Y., Hou Z., Liu Y., 2004, Finite difference time domain method for band-structure calculations of two-dimensional phononic crystals, *Solid State Communications*, **132**, 8, 539-543
3. Chen A.-L., Tian L.-Z., Wang Y.-S., 2017, Band structure properties of elastic waves propagating in the nanoscaled nearly periodic layered phononic crystals, *Acta Mechanica Solida Sinica*, **30**, 2, 113-122
4. Chu J., Zhou G., Liang X., Liang H., Yang Z., Chen T., 2023, A metamaterial for low--frequency vibration damping, *Materials Today Communications*, **36**, 106464
5. Du S., Shi D., Deng H., 2000, Special effects and applications of nanostructured materials, *Nature Magazine*, **22**, 2, 101-106
6. Eringen A.C., Edelen D.G.B., 1972, On nonlocal elasticity, *International Journal of Engineering Science*, **10**, 3, 233-248
7. Ghoreshi M., Bahrami A., 2022, Acoustic invisibility cloak based on two-dimensional solid-fluid phononic crystals, *Solid State Communications*, **342**, 114646
8. Gurtin M.E., Weissmüller J., Larché F., 1998, A general theory of curved deformable interfaces in solids at equilibrium, *Philosophical Magazine A*, **78**, 5, 1093-1109
9. Gurtin M.E., Murdoch I.A., 1975, A continuum theory of elastic material surfaces, *Archive for Rational Mechanics and Analysis*, **57**, 4, 291-323
10. Huang G.-Y., Yu S.-W., 2006, Effect of surface piezoelectricity on the electromechanical behaviour of a piezoelectric ring, *Physica Status Solidi (B)*, **243**, 4, R22-R24
11. Kong D., Wang N., Wang G., Sheng Z., Zhang Y., 2023, Analytical model of vibro-acoustic coupling between the membrane loaded with concentrated masses and the acoustic cavity, *Thin--Walled Structures*, **182**, 110317
12. Lee D., Youn B.D., Jo S.-H., 2023. Deep-learning-based framework for inverse design of a defective phononic crystal for narrowband filtering, *International Journal of Mechanical Sciences*, **255**, 108474

13. Lu J.-F., Cheng J., Feng Q.-S., 2022, Plane wave finite element model for the 2-D phononic crystal under force loadings, *European Journal of Mechanics – A/Solids*, **91**, 104426

14. Qian D., 2018, Bandgap properties of a piezoelectric phononic crystal nanobeam with surface effect, *Journal of Applied Physics*, **124**, 5, 055101

15. Qian D., Shi Z., 2017, Using PWE/FE method to calculate the band structures of the semi-infinite beam-like PCs: Periodic in z-direction and finite in x-y plane, *Physics Letters A*, **381**, 17, 1516-1524

16. Qian D., Zou P., Zhang J., Chen M., 2022, Tunability of resonator with pre-compressed springs on thermo-magneto-mechanical coupling band gaps of locally resonant phononic crystal nanobeam with surface effects, *Mechanical Systems and Signal Processing*, **176**, 109184

17. Sigalas M.M., Economou E.N., 1992, Elastic and acoustic wave band structure, *Journal of Sound and Vibration*, **158**, 2, 377-382

18. Surana K.S., Joy A.D., Reddy J.N., 2017, Non-classical continuum theory for solids incorporating internal rotations and rotations of Cosserat theories, *Continuum Mechanics and Thermodynamics*, **29**, 2, 665-698

19. Yan Z., Jiang L.Y., 2011, The vibrational and buckling behaviors of piezoelectric nanobeams with surface effects, *Nanotechnology*, **22**, 24, 245703

20. Yang F., Chong A.C.M., Lam D.C.C., Tong P., 2002, Couple stress based strain gradient theory for elasticity, *International Journal of Solids and Structures*, **39**, 10, 2731-2743

21. Yang T., Xiao B., Feng Y., Pei D., Liu Y., Chen M., Jiang H., Zheng Z., Wang Y., 2022, Acoustic edge mode in spiral-based metamaterials at subwavelength scale, *Results in Physics*, **42**, 106008

22. Yao L., Zhang D., Xu K., Dong L., Chen X., 2021, Topological phononic crystal plates with locally resonant elastic wave systems, *Applied Acoustics*, **177**, 107931

23. Yin J., Cai L., Fang X., Xiao Y., Yang H., Zhang H., Zhong J., Zhao H., Yu D., Wen J., 2022, Review on research progress of mechanical metamaterials and their applications in vibration and noise control, *Advances in Mechanics*, **52**, 3, 508-586

24. Zhen N., Wang Y.-S., Zhang C., 2012, Surface/interface effect on band structures of nanosized phononic crystals, *Mechanics Research Communications*, **46**, 81-89

25. Zou Y., Wang Z., Adjei P., Zhao X., 2023, The sound insulation performance of light wood frame construction floor structure based on phononic crystal theory, *Journal of Building Engineering*, **75**, 107039

26. Zuo S., Liu P., Wu X., Zhang Q., Kong Y., Zhou D., 2022, Study on broad flexural wave bandgaps of piezoelectric phononic crystal plates for the vibration and noise attenuation, *Thin-Walled Structures*, **178**, 109481

Manuscript received August 8, 2023; accepted for print September 27, 2023